Design, Modeling, and Validation of a Self-Balancing Cable-Driven Continuum Robot Using Internal Force Equilibrium

Ammar Amouri
Professor
Department of Mechanical Engineering
Laboratory of Mechanics, Frères Mentouri
Constantine 1 University
Algeria

Omar Rahma
PHD Student
Department of Mechanical Engineering
Laboratory of Mechanics, Frères Mentouri
Constantine 1 University
Algeria

Ensuring effective operation is crucial for continuum robots, especially in tasks requiring precision under varying external loads. This study introduces a Self-Balancing Cable-Driven Continuum Robot (SB-CDCR) designed to minimize vibrations and enhance mechanical stability, defined here as the robot's ability to maintain shape, resist deformation, and suppress oscillations during motion. The initial robot design consists of three modules, each composed of adjacent disk pairs interconnected by four springs: one central compression spring for axial support and three lateral tension springs for passive balancing. The proposed design integrates several key features, including a lightweight structure, high flexibility, and reinforced internal support. This configuration, combined with a pre-stressed internal force distribution, ensures smooth motion, vibration suppression, and improved structural integrity, thereby enabling precise control of spatial movements. Kinematic models are developed using the Constant Curvature (CC) approach, allowing the analytical formulation of forward kinematics and workspace analysis.The inverse kinematics is addressed as a quadratic optimization task and is effectively solved using the Weighted Particle Swarm Optimization (W-PSO) algorithm. Numerical simulations demonstrate accurate trajectory tracking with a positional error of 2.616×10^{-3} *mm and a computation time of* 3.954 *ms. Experimental validations further confirm the robot's accuracy under load-handling conditions.*

.

Keywords: *Continuum robot, cable-driven continuum robot, kinematic modeling, positional accuracy, load capacity analysis..*

1. INTRODUCTION

Continuum robots have attracted increasing attention due to their outstanding flexibility, dexterity, and intrinsic compliance, enabling safe and effective interaction with complex or unstructured environments. These features arise from their continuous, lightweight structures that can bend, extend, and contract along their length, surpassing traditional rigid-link manipulators in confined or delicate tasks.

Recent advances in continuum robotics have led to a wide variety of designs, including both soft and cable-driven structures. Soft continuum robots, typically actu–ated pneumatically, rely on compliant materials and include examples such as the Compact Bionic Handling Arm [1], the Bionic Handling Arm [2], and other bio-inspired systems [3,4]. In contrast, Cable-Driven Conti–nuum Robots (CDCRs) employ diverse backbone and actuation mechanisms, including single or multiple cen–tral springs [5,6], flexible rods [7,8], sheet-based struc–tures [9,10], segmented joints [11], sliding disks [12], notched superelastic tubes [13], and concentric pre-bent tubes [14]. Their actuation principles include cable or tendon systems [7–10], shape-memory materials [15], and motor-based hybrid actuation [14].

However, conventional CDCRs often suffer from insufficient structural stability, which limits their positi–oning accuracy, load capacity, and overall performance. In this context, structural stability is defined as the robot's ability to maintain its intended shape and orien–tation under internal cable tensions and external distur–bances. Unbalanced internal forces or uneven stiffness distribution can cause undesired deflections, vibrations, or even buckling, leading to degraded motion perfor–mance. For cable-driven continuum robots, structural stability thus includes both axial stiffness (resistance to compression and extension) and lateral equilibrium (resistance to asymmetric bending and shape distortion).

Previous studies have often relied on increasing backbone rigidity or implementing active feedback control to improve stability. However, these approaches often introduce additional system complexity, require extra sensors, and may not fully prevent undesired vibrations or shape deformations under varying loads. Furthermore, few studies address the distribution of internal forces in a way that ensures passive self-stabilization. These deficiencies highlight the need for a mechanically robust solution that can maintain equilibrium without relying on active control. To add–ress these challenges, the proposed Self-Balancing

Received: December 2025, Accepted: January 2026
Correspondence to: Pr. Ammar Amouri
Department of Mechanical Engineering, Frères Mentouri Constantine 1 University, Algeria.
E-mail: ammar_amouri@yahoo.fr
doi: 10.5937/fme2601117A

Cable-Driven Continuum Robot (SB-CDCR) introduces a novel spring-based internal force equilibrium mecha–nism. By incorporating preloaded central and lateral springs, the SB-CDCR achieves uniform internal force distribution, passive self-balancing, and enhanced struc–tural stability. This design ensures precise spatial posi–tioning even under varying loads, making the robot par–ticularly well-suited for applications that require accu–rate and adaptable manipulation in confined or cluttered environments, such as biomedical procedures [16] and industrial inspections [17]. In addition, its modular structure and intrinsic self-balancing mechanism enable manipulation of fragile objects [18], extension to multi-section configurations for complex three-dimensional tasks, and operation in environments where additional sensors or active control are limited [19]. Overall, the SB-CDCR combines intrinsic stability, high positional accuracy, and a compact structure, representing a signi–ficant step toward mechanically self-stabilizing conti–nuum robots with practical engineering applications.

The SB-CDCR is composed of three interconnected modules, each consisting of a pair of adjacent disks con–nected by a central compression spring and three sym–metrically arranged lateral tension springs. The central spring provides axial stiffness and acts as the backbone, counteracting compression and external dis–turbances, while the lateral springs maintain balance and enhance rigidity by uniformly distributing tension around the central axis. This self-balancing configuration allows the springs to work cooperatively, maintaining the desired shape and minimizing undesired deformations during operation. As a result, the robot exhibits improved stiff–ness, vibration damping, and shape retention compared to conventional cable-driven designs. Moreover, the modular structure of the SB-CDCR can be extended to form a multi-section conti–nuum robot, offering inc–reased flexibility and enabling more complex three-dimensional motion for advanced manipulation tasks.

While both cable-driven actuation and spring-based backbones are well-established in continuum robotics, the novelty of the proposed SB-CDCR lies in its intrinsic self-balancing mechanism. Unlike previous de–signs that rely on feedback control or enhanced struc–tural rigidity to improve stability, the SB-CDCR achi–eves equilibrium through passive internal force distri–bution among the central and lateral springs. This configuration enables the robot to maintain structural integrity and stability without additional sensors or active compensation, representing a distinct step toward mechanically self-stabilizing conti–nuum robot architectures.

A rigorous understanding of this mechanical beha–vior is essential for accurate modeling, motion analysis, and control. Kinematic modeling defines the relation–ship between the end-effector pose and the robot's configuration or actuator parameters, without consi–dering inertia and external loads. However, due to the continuum nature of these robots, the derivation of precise kinematic models remains challenging because of their deformable structures, complex actuation, and nonlinear geometric behavior.

Several alternative methods have been explored in the literature to address continuum robot kinematics, including the modal approach [20], geometric arc for–mulation [21], beam and Cosserat-rod theories [22,23], elliptic integral modeling [24], and hybrid model-learning strategies [1]. Other curve-based represen–tations, such as serpenoid and clothoid shapes, have also been investigated [25,26]. Each method presents advantages and limitations depending on the robot's geometry, de–sired accuracy, computational efficiency, and control objectives. Nevertheless, solving the inverse kinematics problem for continuum robots remains highly challenging due to their inherently deformable structures, high redundancy, coupled multi-section mo–tion, and nonli–near geometric behavior. Traditional aalytical or iterative methods often fail to converge or require heavy simp–lifications that compromise accuracy. In this work, the inverse kinematics problem is formulated as a quadratic optimization task, providing a flexible framework to handle constraints and nonlinearity. Like all optimization problems, this one can be addressed using various metaheuristic algorithms such as Genetic Algorithm (GA) [27], Grey Wolf Optimization (GWO) [28], Differential Search Algorithm (DSA) [29], and Artificial Bee Colony (ABC) [30]. In this study, the Weighted Particle Swarm Optimization (W-PSO) algorithm [31] is employed due to its ability to efficiently handle nonlinearities, high-dimensional search spaces, and multiple constraints with minimal parameter tuning.

To simplify the modeling process while preserving analytical tractability, the Constant Curvature (CC) assumption [32] is adopted in this study. This assum–ption enables the derivation of an efficient forward kinematic model and facilitates the workspace analysis of the proposed SB-CDCR.

The main contributions of this paper are summarized as follows:

Presentation and structural analysis of the Self-Balancing Cable-Driven Continuum Robot (SB-CDCR).

Development of a forward kinematic model based on the Constant Curvature (CC) assumption.

Solution of the inverse kinematic problem using the Weighted Particle Swarm Optimization (W-PSO) algorithm.

Investigation of the workspace and load-handling capability of the SB-CDCR..

Evaluation of the robot's positional accuracy and load-carrying performance through simulation and experimental validation.

The remainder of the paper is organized as follows: Section 2 presents a detailed explanation of the mechanical design and describes the fabrication process. Section 3 is devoted to the development of the kinematic model for the proposed robot. In Section 4, simulation results are presented to validate the inverse kinematic model and to generate the workspace of the SB-CDCR. Section 5 describes the experimental tests conducted to assess the robot's positional accuracy and load handling capability. Finally, Section 6 summarizes the findings and outlines prospects for future research.

2. DESIGN AND PROTOTYPE DEVELOPMENT OF SB-CDCR

The Self-Balancing Cable-Driven Continuum Robot (SB-CDCR) consists of three interconnected modules,

each formed by two disks connected through a central compression spring and three lateral tension springs, as shown in Figure 1. The central spring provides axial resistance, acting as the backbone and primary support of the robot, counteracting external forces. Meanwhile, the lateral springs, positioned at 120° intervals, enhance rigidity and stability. This configuration ensures smooth motion and minimizes vibrations, enabling precise control of spatial movements. By adjusting the tension in one, two, or all three cables, the robot can bend, rotate, and retract as needed, as depicted in Figure 2.

During assembly, each module is preloaded to establish a stable equilibrium. The central spring is initially compressed between the two disks, while the lateral springs are extended to generate opposing forces before being manually installed on the appropriate faces of the disks. After assembling the three modules onto the base, the drive cables are threaded through the slots in the disks and base. This pre-stressed internal force distribution minimizes deformations, enhances structural integrity, and dampens oscillations, resulting in improved motion precision. It is important to note that, in this context, the term "self-balancing" refers to the robot's inherent ability to maintain uniform support and suppress unwanted vibrations under dynamic conditions.

The manufacturing process began with 3D printing key components, including the base and three disks, using a Zortrax M300 Plus 3D printer. Once fabricated, these components were assembled to construct the SB-CDCR. The robot has three degrees of freedom, comprising one translational and two rotational movements. Its flexible arm, weighing 0.117 kg, can extend from 130 mm to 200 mm. This design enables a bending range of $\pm\pi/2$ and an orientation range from 0 to 2π, allowing for controlled three-dimensional motion.

3. KINEMATICS MODELING

3.1 Modeling assumptions

Modeling continuum robots is challenging, especially in accurately mapping the relationship between actuator space and task space without approximations. Their complex characteristics, including redundancy and non–linearities, further complicate the modeling process, beyond basic structural or behavioral considerations. These challenges make it difficult to create a comprehensive model without specific assumptions. To overcome these challenges, the following assumptions are made in this paper:

- The robot's bending profile follows a constant circular arc.
- The springs are modeled according to Hooke's law, with no energy dissipation.
- Each spring has a uniformly distributed mass along its length.
- The lateral springs between adjacent disks are modeled as straight lines, while the central spring forms a circular arc.
- The driving cables are considered inextensible.
- Torsional effects in the springs are neglected.

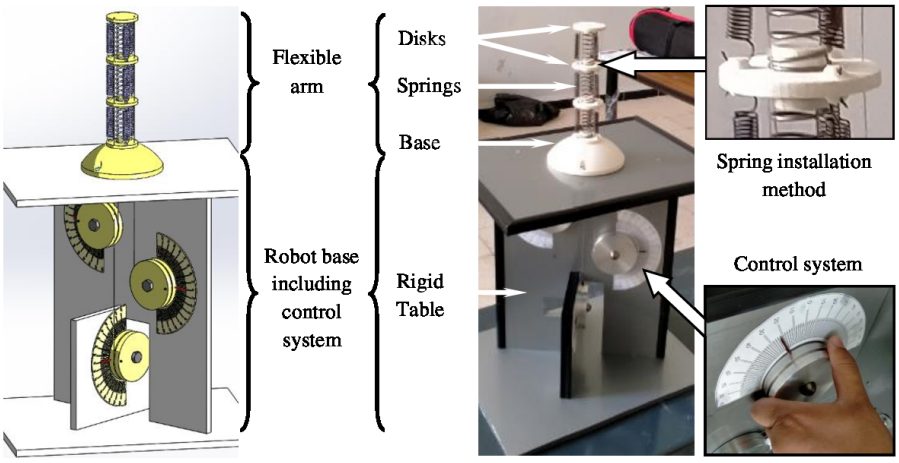

Figure 1. Structure of the Self-Balancing Cable-Driven Continuum Robot (SB-CDCR) and its main components: (a) three-dimensional CAD model; (b) initial physical prototype

Figure 2. Configurations of the SB-CDCR: (a) initial configuration with zero cable tension; (b) retraction and bending configuration, with all three cables actuated and differential tension applied among them; (c) bending configuration with one or two cables actuated simultaneously; (d) suboptimal bending configuration

Under these assumptions, the bending behavior of each section can be represented by a constant curvature profile, a common simplification in continuum robot modeling. Although the SB-CDCR consists of a curved central compression spring and straight lateral tension springs, this assumption remains valid within moderate deformation ranges, where the bending of each module can be approximated as a circular arc. This simplification allows for an accurate estimation of the end-effector position and orientation while keeping the analytical formulation manageable. However, it is acknowledged that at larger deflection angles or under high external loads, deviations from the constant curvature behavior may occur due to non-uniform spring stiffness and asymmetric cable tensions.

3.2 Forward kinematic modeling

Relying on the above assumptions, the Constant Curvature (CC) method [32] is employed to derive the forward kinematic model of the proposed SB-CDCR, which defines the distal tip pose H relative to the robot's base. The derivation proceeds in two main steps. First, the distal tip pose is expressed in terms of the configuration parameters; namely the arc length s, bending angle θ, and orientation angle φ, as illustrated in Figure 3. The corresponding homogeneous transformation matrix H is formulated as:

$$\mathrm{H}=\begin{bmatrix}\mathrm{R}_{3\times3} & \mathrm{x}_{3\times1}\\ 0_{1\times3} & 1\end{bmatrix}, \tag{1}$$

where the rotation matrix R and the position vector $\mathrm{x}=\{x,y,z\}^{\mathrm{T}}$ are defined as:

$$\mathrm{R}=\mathrm{rot}(z,\varphi)\cdot\mathrm{rot}(y,\theta)\cdot\mathrm{rot}(z,-\varphi), \tag{2}$$

$$\mathrm{x}=\left\{\frac{s\left(1-\mathrm{c}(\theta)\right)\mathrm{c}(\theta)}{\theta},\frac{s\left(1-\mathrm{c}(\theta)\right)\mathrm{s}(\theta)}{\theta},\frac{s\mathrm{s}(\theta)}{\theta}\right\}^{\mathrm{T}}, \tag{3}$$

in these equations, the rot(u,ξ) denotes a (3×3) rotation matrix about the axis u by the angle ξ, and the functions c(·) and s(·) represent the cosine and sine functions, respectively. it is important to note that in equation (3), the bending angle θ appears in the denominator, leading to mathematical singularities when the robot is fully extended or retracted (i.e., when $\theta = 0$). to resolve this issue, an asymptotic substitution is applied as the bending angle approaches zero.

The second step involves obtaining the configuration parameters as a function of the actuation cable lengths, expressed as follows:

$$\mathrm{x}=\begin{cases}s=\dfrac{1}{3}\left(l_1+l_2+l_3\right)\\ \theta=\dfrac{\sqrt{l_1^2+l_2^2+l_3^2-l_1l_2-l_1l_3-l_2l_3}}{3r}\\ \varphi=\tan^{-1}\left(\dfrac{\sqrt{3}\left(l_3-l_2\right)}{2l_1-l_2-l_3}\right)\end{cases}, \tag{4}$$

where r denotes the radial distance between the virtual central axis of the SB-CDCR and the cables.

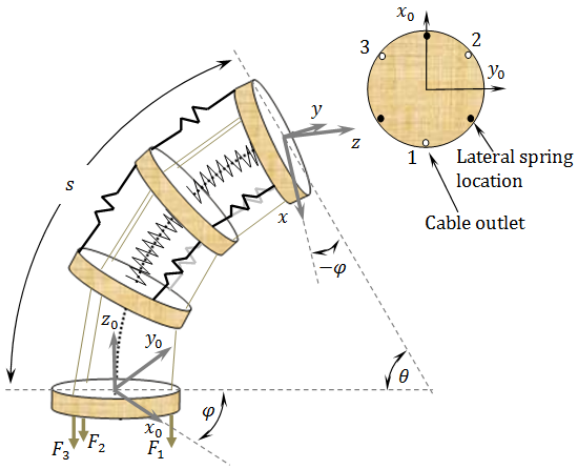

Figure 3. Schematic of the SB-CDCR showing its configuration parameters, along with the arrangement of the actuator cables and lateral springs

3.3 Inverse kinematic modeling

The inverse kinematic model of the Self-Balancing Cable-Driven Continuum Robot (SB-CDCR) is highly complex, making it impractical to derive an analytical solution for determining the cable lengths l_1, l_2, and l_3 in terms of the target coordinates x, y, and z. The equations are strongly nonlinear, involving trigonometric functions and square root terms. Moreover, the cable lengths are interdependent on the angular variables variables θ and φ, resulting in a coupled nonlinear system. To overcome this complexity, metaheuristic optimization techniques are required.

Metaheuristic optimization techniques are general-purpose algorithms inspired by natural, biological, or social processes, designed to find near-optimal solutions for complex optimization problems. Their principle is to explore the search space efficiently and iteratively improve candidate solutions**,** often balancing global exploration (searching broadly) and local exploitation (refining promising areas). Among these, commonly applied techniques include Genetic Algorithms (GAs) [27], Grey Wolf Optimization (GWO) [28], Differential Search Algorithm (DSA) [29], Artificial Bee Colony (ABC) [30], and Weighted Particle Swarm Optimization (W-PSO) algorithm [31], among others.

Genetic Algorithms (GAs) use selection, crossover, and mutation operators, offering strong global exploration, though they may require careful parameter tu–ning and can converge more slowly in smooth conti–nuous problems. Grey Wolf Optimization (GWO) mimics social hierarchy and hunting behavior, balan–cing exploration and exploitation, but convergence speed can vary depending on the number of wolves and initial distributions. Artificial Bee Colony (ABC) is robust to local minima and well-suited for multimodal optimization, though it may need more iterations to achieve high precision. Differential Search Algorithm (DSA) uses population-based differential operations to explore the search space, but scaling and step-size parameters must be tuned for rapid convergence in high-dimensional problems.

To address these challenges, the Weighted Particle Swarm Optimization (W-PSO) algorithm is employed. W-PSO extends the standard PSO [33–35] by introducing an inertia weight, which enables adaptive balancing between global exploration and local exploitation. This mechanism improves convergence stability, prevents premature stagnation around local minima, and ensures robust performance across different initial particle distributions. The choice of W-PSO over other metaheuristic optimization techniques is justified by its relatively fast convergence, reduced sensitivity to parameter tuning, and high accuracy in solving nonlinear inverse kinematic problems, which is particularly important for handling the coupled nonlinearities of the SB-CDCR.

A flowchart illustrating the iterative optimization process is presented in the algorithm below. In W-PSO, the particle positions represent the decision variables of the optimization problem, which, in this case, correspond to the Cartesian coordinates of the end-effector points. Moreover, the population in W-PSO consists of all possible candidate solutions for this optimization problem. Since the performance of an optimization algorithm largely depends on parameter tuning, the parameters used for the W-PSO algorithm in the following section are summarized in Table 1. The simulations were carried out using MATLAB on a system equipped with an Intel® Core™ i3-2310M CPU (2.10 GHz) and 4 GB of RAM.

Algorithm : Flowchart of the W-PSO

1: Start: Initialize the parameters, swarm size, and positions.

2: Generate target trajectory: Define the desired *x, y, z* target position.

3: Evaluate forward kinematics: Compute the robot's current position based on particle states, using Equations 3 and 4.

4: Calculate Cost function: Determine the error between the current and target positions, using the quadratic cost function $C_f = ||x - x_{target}||^2$, where x is the current position of the robot (based on the state of the particle p), and x_{target} is the desired target position.

5: Update best values: Adjust personal and global bests based on the cost function.
- Personal Best: $P^{best} = P_p$ if $C_f < C_{f,previous}$.
- Global Best: $G^{best} = P^{best}$ if $C_f < C_{f,global}$.

6: Update velocities and positions: Modify particle velocities and positions for the next iteration:
- Velocity:

$$v_{t+1}^p = \omega v_t^p + c_1\rho_1\left(P^{\text{best}} - x_t^p\right) + c_2\rho_2\left(G^{\text{best}} - x_t^p\right)$$

- Position: $x_{t+1}^p = x_{t+1}^p + v_{t+1}^p$

where v_t^p is the velocity of particle p, ω is the inertia weight, c_1 and c_2 are cognitive and social scaling factors, respectively, and ρ_1 and ρ_2 are random numbers.

7: Check stopping criterion: Determine if the maximum iterations or acceptable error is reached.

8: Output optimal solution: Provide the best cable lengths for the target.

Table 1. Weighted Particle Swarm Optimization parameters

Swarm size	Iterations	ω	c_1	c_2
25	100	0.695	0.9925	0.9925

4. KINEMATIC SIMULATION RESULTS

4.1 Simulation analysis of the SB-CDCR's workspace

To generate a trajectory that the robot can accurately follow, it is essential to have a clear understanding of its workspace, which consists of all positions reachable by its end-tip. Figure 4 provides a visual representation of potential end-tip positions of the SB-CDCR in both two- and three-dimensional forms. These positions were determined using the forward kinematic model and the parameters outlined in Section 2. In the Figures, the end-tip positions associated with the minimum and maximum cable lengths are denoted by points A and B (solid red circles). The gray region enclosed between the curved black boundary (C) and the blue boundary (D) defines the reachable workspace of the SB-CDCR.

4.2 Simulation of point-to-point trajectory tracking

In this subsection, two simulation examples are presented for point-to-point trajectory tracking. The first simulation involves tracking a vertical line-shaped trajectory, while the second focuses on a complex spiral-shaped trajectory. In both cases, the robot starts from an initial state of $x = [0, 0, 200]^T$ mm. The results illustrate the inverse kinematic model solution of the SB-CDCR using the W-PSO algorithm, including the desired and generated trajectories, Euclidean errors along the axes, and execution times, as shown in Figures 5 and 6, respectively. Additionally, Figures 7 and 8 illustrate the variations in cable lengths, bending angles, and orientation angles required to track the trajectories. A summary of the average results is presented in Table 2.

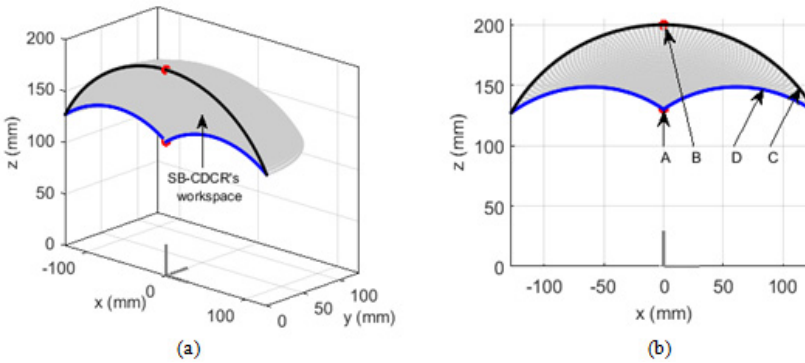

Figure 4. Representations of the SB-CDCR workspace. (a) half-perspective three-dimensional view, and (b) two-dimensional view

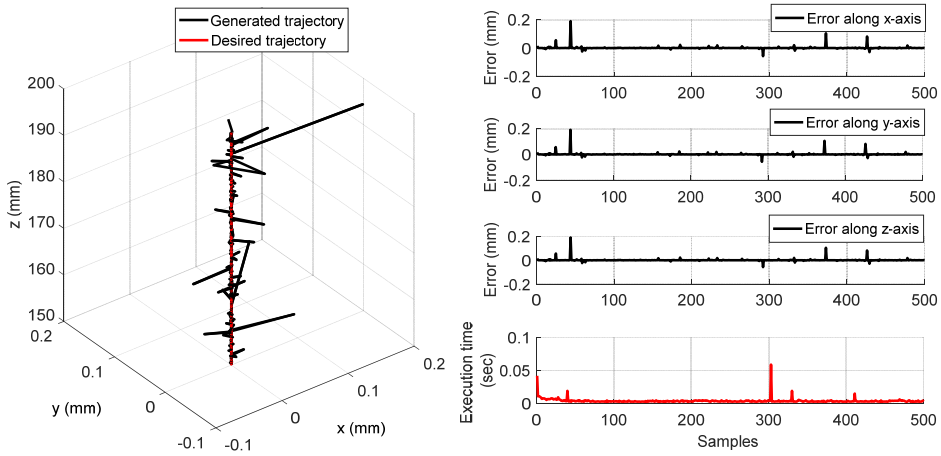

Figure 5. Desired and generated vertical line-shaped trajectory with Euclidean errors and execution time

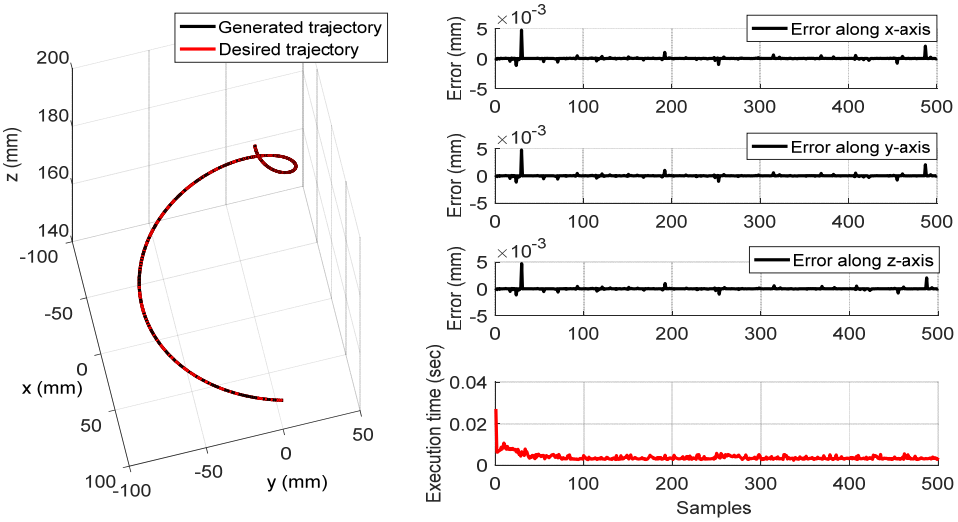

Figure 6. Desired and generated complex spiral-shaped trajectory with Euclidean errors and execution time

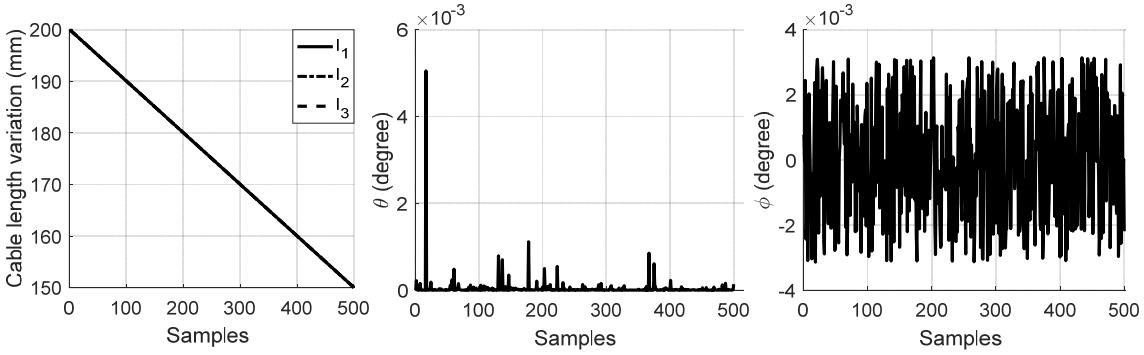

Figure 7. Cable length variations, along with the bending angle and orientation angle, required for tracking the vertical line-shaped trajectory

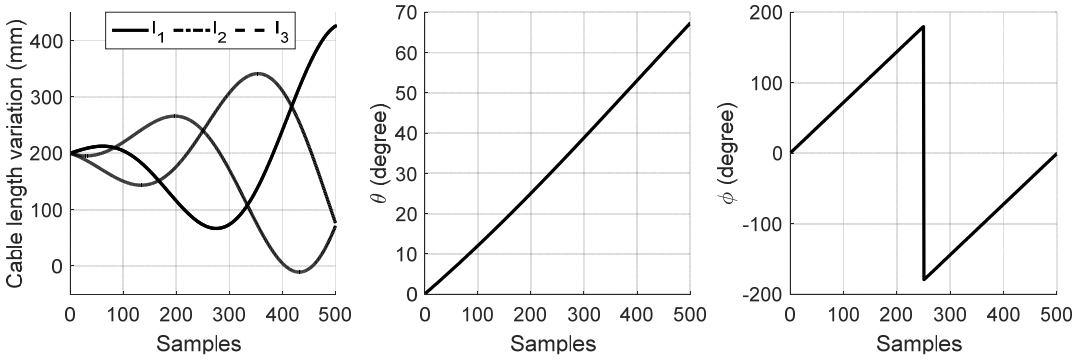

Figure 8. Cable length variations, along with the bending angle and orientation angle, required for tracking the complex spiral-shaped trajectory

Table 2: Key results of the simulated SB-CDCR for trajectory tracking

Simulation	Mean Error (mm)	Mean execution time (ms)
Line-shaped trajectory	$2.616 \cdot 10^{-3}$	3.954
Spiral-shaped trajectory	$1.084 \cdot 10^{-4}$	3.919

From Table 2, it can be observed that the application of the W-PSO algorithm yields excellent results in terms of both trajectory tracking accuracy and execution time. The low mean error values and fast execution times for both the line-shaped and spiral-shaped trajectories demonstrate the efficiency and reliability of the algorithm. Based on these results, the W-PSO algorithm proves to be a promising approach for solving the inverse kinematics of the SB-CDCR, ensuring precise tracking performance while maintaining computational efficiency.

5. EXPERIMENTAL STUDY

5.3 Experimental setup

In order to validate the design principle, experimental tests were conducted on the considered robot to examine its deformation with and without an external load. Given the lightweight nature of the robot, the aim of this study is to confirm the feasibility of using the Constant Curvature (CC) approach [31] for modeling, thereby validating the developed kinematic models. Additionally, these experimental results help verify design specifications and enhance the robot's reliability by understanding its load-bearing limits, allowing for necessary adjustments in future work.

The test bench, depicted in Figure 9, comprises the following components:

- Self-Balancing Cable-Driven Continuum Robot (SB-CDCR): primary subject of the load capacity tests.
- Rigid support table: contains the manual control system for operating the robot.
- Portable 3D Measuring Arm (Romer Absolute Arm, Model RA-7312): serves as a crucial element for precise measurements in the experimental setup, with a measurement accuracy of approximately ±20 μm.

Before initiating the measurement process, the reference frame of the portable 3D measuring arm was aligned with the fixed frame of the robot. Subsequently, the pose of the SB-CDCR end-tip was adjusted by manipulating the lengths of the actuating cables, achieved through manual rotation of the pulleys. This process is illustrated in the zoomed-in panel of Figure 9, which depicts the control system.

Throughout each case study and measurement process, the Cartesian coordinates of the SB-CDCR's end-tip were documented and stored using the portable 3D measuring arm, with measurements acquired via a PC. Simultaneously, changes in cable length for the SB-CDCR were measured and manually recorded after performing simple transformations.

5.4 Validation of the CC approach for SB-CDCR modeling under free-loading conditions

Experimental evaluations of the SB-CDCR end-tip without external loads were conducted across four distinct configurations, as shown in Figure 10. These configurations include: vertical placement with the free end oriented upward (Conf_VH), horizontal placement with upward curvature (Conf_HH), vertical placement with the free end oriented downward (Conf_VB), and horizontal placement with downward curvature (Conf_HB).

Figure 11 illustrates a comparison between the simulation results obtained using the CC approach and the experimental measurements for the four configurations. The analysis shows an acceptable correlation between the experimental data and the curve generated by the CC approach, with a maximum mean error of 1.762 mm, representing only 0.881% of the robot's total length. This result highlights the precision and reliability of the CC approach in modeling the SB-CDCR under free-loading conditions.

Despite the observed accuracy, several factors contribute to measurement uncertainties, including: (i) potential misalignment during the initial setup of the prototype and the portable 3D measuring arm; (ii) inconsistencies in manually positioning the arm probe on the marker points during data collection, and (iii) manufacturing tolerances of the prototype.

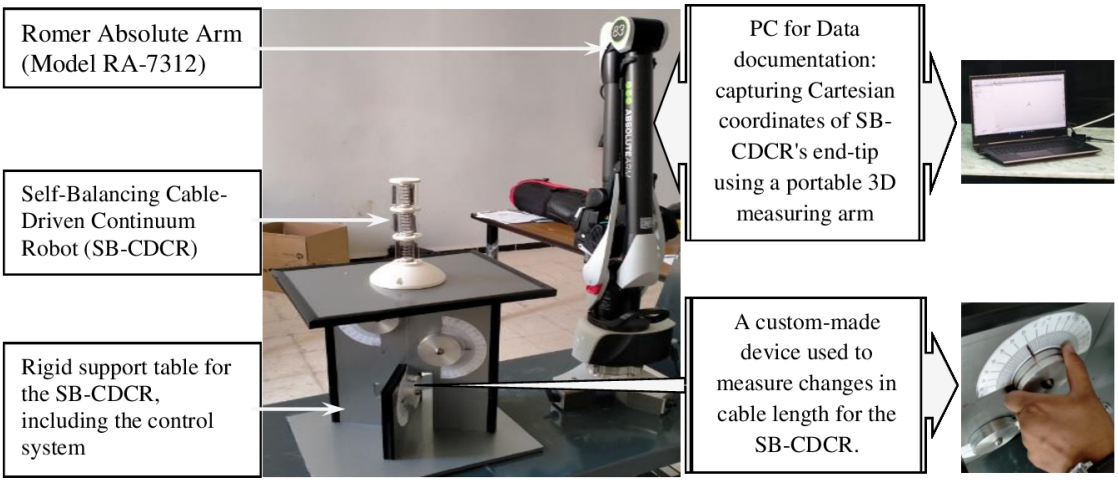

Figure 9: Overview of the test bench

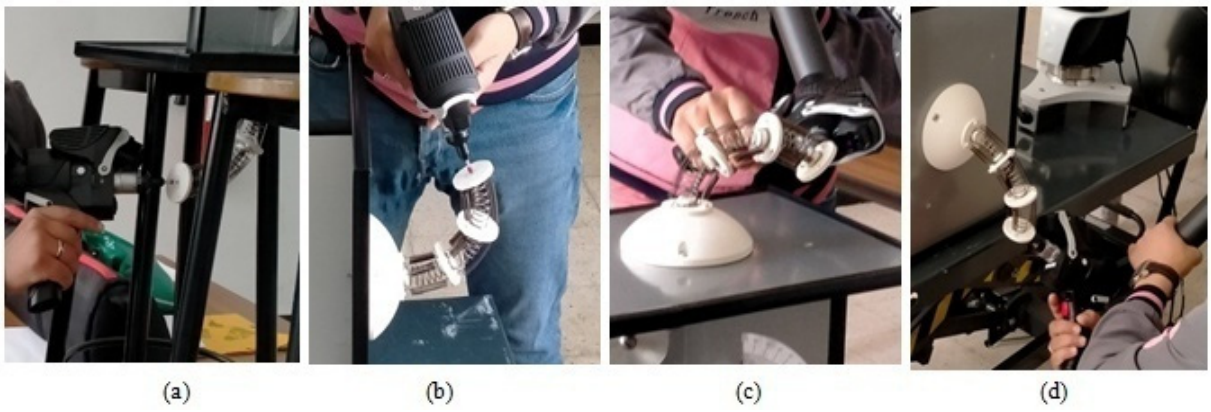

Figure 10: Experimental configurations (a) Conf_VH, (b) Conf_HH, (c) Conf_VB, and (d) Conf_HB

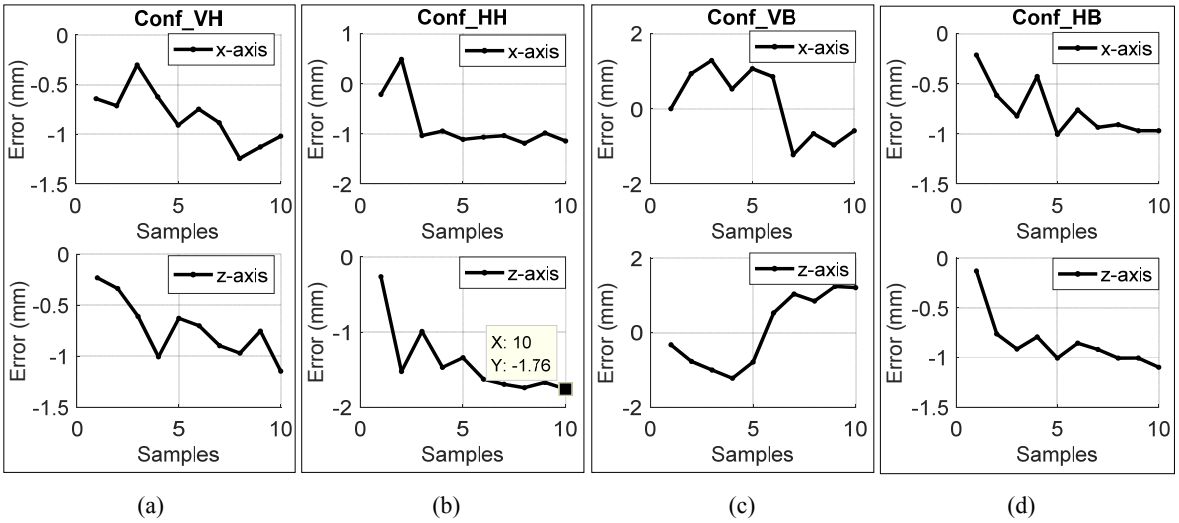

Figure 11: Comparison of CC approach simulation results and experimental measurements for SB-CDCR end-tip configurations under free-loading conditions: (a) deviations along *x* and *z* for Conf_VH, (b) Conf_HH, (c) Conf_VB, and (d) Conf_HB

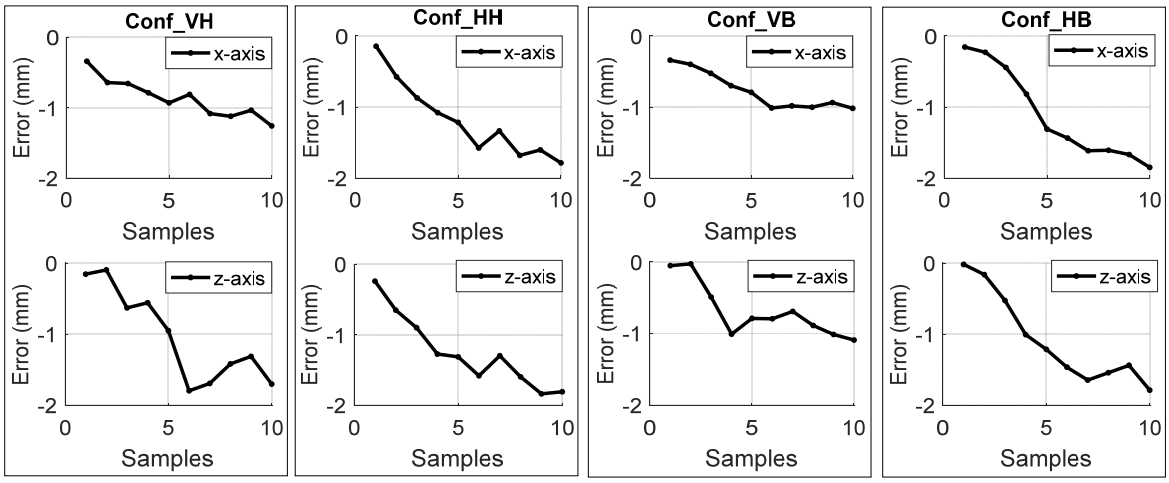

Figure 12: **Comparison between CC approach simulation results and experimental measurements for SB-CDCR end-tip configurations under a 50 g external load: (a) Deviations along x and z for Conf_VH, (b) Conf_HH, (c) Conf_VB, and (d) Conf_HB.**

5.5 Load experiment on various robot configura–tions under an external load

The same configurations presented in Figure 10 were analyzed under the influence of an external load of 50 g applied to the free end-tip of the SB-CDCR. Given that the CC approach has demonstrated its accuracy in modeling the SB-CDCR, it can now serve as a reference for this analysis. Figure 12 compares the simulation results of the CC approach with the experimental mea–surements across the four robot configurations under the applied external load.

The results indicate that configuration errors bet–ween simulation and experimental measurements vary depending on the axes and tested configurations under a 50 g load. In Conf_VH, errors on the x – axis gradually

increase to 1.258 mm, while those on the *y*-axis fluc–tuate more irregularly, reaching 1.795 mm. For Conf_HH, errors peak at 1.488 mm and 1.413 mm on the *x*- and *y*-axes, respectively, likely due to geometric complexity. In Conf_VB, maximum errors are 1.018 mm (*x*-axis) and 1.091 mm (y-axis), indicating better alignment between the model and reality. Lastly, in Conf_HB, errors reach 1.148 mm and 1.191 mm along the *x*- and *z*-axes, showing relative consistency despite persistent deviations. These findings highlight the vari–ability of errors across configurations, with generally higher accuracy in vertical scenarios compared to hori–zontal ones. Overall, the results demonstrate that the robot can support its own weight and handle lightweight loads.

It should be noted that the present experimental study was primarily designed to validate the kinematic modeling accuracy of the SB-CDCR under both unlo–aded and loaded conditions. While the self-balancing design concept inherently contributes to improved internal force equilibrium and reduced susceptibility to oscillations, the quantitative evaluation of dynamic stability and vibration suppression remains beyond the current experimental scope. Future work will therefore include dynamic characterization tests, such as transient response analysis and oscillation damping measure–ments, to provide further evidence supporting the ro–bot's self-stabilizing behavior under time-varying conditions.

6. CONCLUSION

This paper presents the design, kinematic modeling, and workspace analysis of a novel Self-Balancing Cable-Driven Continuum Robot (SB-CDCR) and evaluates its positional accuracy and load capacity across various configurations. A detailed description of the robot's design and prototyping is provided, highlighting its principal components. The proposed SB-CDCR offers notable advantages, including a lightweight structure, stable deformation during motion, and vibration-free operation, distinguishing it from conventional CDCRs. In particular, the modular architecture with preloaded central and lateral springs ensures an inherent internal force equilibrium, significantly enhancing structural stability and vibration suppression without the need for active control, making it suitable for practical imple–mentation. The forward kinematic model is developed using the Constant Curvature (CC) approach, and the robot's workspace is comprehensively analyzed. Given the nonlinear nature of the forward kinematic model, the inverse kinematic problem is formulated as an optimi–zation task with a quadratic cost function and solved using the Weighted Particle Swarm Optimization (W-PSO) algorithm.

Numerical examples of point-to-point trajectory tracking are presented to demonstrate the effectiveness of the W-PSO algorithm. Furthermore, experimental measurements, both with and without applied loads, validate the Constant Curvature (CC) approach used in modeling the SB-CDCR and assess the design's key principles as well as the robot's load-carrying capacity. Based on the simulation results, the algorithm achieves a positional accuracy of $2.616 \cdot 10^{-3}$ mm with a compu–tational time of 3.954 ms. A key strength of W-PSO lies in its ability to manage the highly nonlinear and coupled nature of the inverse kinematics, which is challenging to solve analytically. Moreover, compared to several com–monly used metaheuristic algorithms, it requires only a few tuning parameters, enhancing ease of implemen–tation and robustness. Validation experiments under free-loading conditions in four configurations, show strong agreement with the CC model, with a maximum mean error of 1.762 mm (0.881% of the robot's total length). However, by averaging the errors across the four configurations, the mean error is 0.519 mm, cor–responding to only 0.2595% of the robot's total length. Under an external load applied at the free end, the mean positional errors for these configurations remain below 1.5 mm (less than 0.75% of the robot's total length), with configuration-specific maxima reaching 1.795 mm. In view of the obtained results, the proposed SB-CDCR demonstrates excelent self-balancing capability and structural stability under both unloaded and loaded conditions. Meanwhile, the W-PSO algorithm highlights its robustness and effectiveness in trajectory tracking, achieving high positional accuracy and fast computa–tional performance.

Future research will explore several directions aimed at enhancing the design and dynamic modeling of the SB-CDCR. From a design perspective, further studies will focus on optimizing structural parameters, parti–cularly the stiffness ratio between the central compres–sion spring and the lateral tension springs, to achieve an optimal balance between flexibility, vibration supp–ression, and structural integrity. Experimental vibration tests will also be conducted to assess the damping characteristics and validate the self-balancing perfor–mance of the proposed configuration under dynamic conditions. In terms of modeling, a comprehensive dynamic model will be developed to account for ex–ternal disturbances, spring nonlinearities, and frictional effects, thereby improving prediction accuracy and enabling more precise control. These investigations will further consolidate the self-balancing design concept and expand the potential applications of the SB-CDCR in advanced manipulation and adaptive robotic systems.

REFERENCES

[1] Lakhal, O., Melingui, A., Merzouki, R.: Hybrid approach for modeling and solving of kinematics of a compact bionic handling assistant manipulator, IEEE/ASME Trans. Mechatronics Vol. 21, No. 3, pp. 1326–1335, 2016.

[2] Mahl, T., Hildebrandt, A., Sawodny, O.: A variable curvature continuum kinematics for kinematic control of the bionic handling assistant, IEEE Trans. Robot, Vol. 30, No. 4, pp. 935–949, 2014.

[3] Qin, L., Peng, H., Huang, X., et al.: Modeling and simulation of dynamics in soft robotics: a review of numerical approaches, Curr. Robot. Rep, Vol. 5, pp. 1–13, 2024.

[4] Talas, S.K., Baydere, B.A., Altinsoy, T., et al.: Design and development of a growing pneumatic soft robot, Soft Robot, Vol. 7, pp. 521–533, 2020.

[5] Gao, G., Wang, H., Liu, J., et al.: Statics analysis of an extensible continuum manipulator with large deflection, Mech. Mach. Theory, Vol. 141, No. 245–266, 2019.

[6] Yoon, H.S., Yi, B.J.: A 4-DOF flexible continuum robot using a spring backbone, in: Proc. Int. Conf. Mechatronics Autom., Changchun, China, pp. 1249–1254, 2009.

[7] Rone, W.S., Ben-Tzvi, P.: Mechanics modeling of multi-segment rod-driven continuum robots, J. Mech. Robot, Vol. 6, No. 4, pp. 69–73, 2014.

[8] Bousbia, L., Amouri, A., Cherfia, A.: Dynamic modeling of a 2-DoFs cable-driven continuum robot, World J. Eng., Vol. 20, No. 4, pp. 631–640, 2023.

[9] Zhou, P., Yao, J., Zhang, S., et al.: A bioinspired fish-bone continuum robot with rigid-flexible-soft coupling structure, Bioinspir. Biomim., Vol. 17, No. 6, 2022.

[10] Amouri, A., Cherfia, A., Belkhiri, A., et al.: Bio-inspired novel dual-cross-module sections cable-driven continuum robot: design, kinematics mode–ling and workspace analysis, J. Braz. Soc. Mech. Sci. Eng., Vol. 45, 2023.

[11] Huang, S., Meng, D., She, Y., et al.: Statics of con–tinuum space manipulators with nonconstant cur–vature via pseudorigid-body 3R model, IEEE Access, Vol. 6, pp. 70854–70865, 2018.

[12] Troncoso, D.A., Robles-Linares, J.A., Russo, M., et al.: A continuum robot for remote applications: from industrial to medical surgery with slender continuum robots, IEEE Robot. Autom. Mag., Vol. 30, No. 3, pp. 94–105, 2022.

[13] Murphy, R.J., Kutzer, M.D.M., Segreti, S.M., et al.: Design and kinematic characterization of a surgical manipulator with a focus on treating osteolysis, Robotica, Vol. 32, No. 6, pp. 835–850, 2014.

[14] Mitros, Z., Sadati, S.H., Henry, R., et al.: From the–oretical work to clinical translation: progress in concentric tube robots, Annu. Rev. Control Robot. Auton. Syst., Vol 5, pp. 335–359, 2022.

[15] Bishop, C., Russo, M., Dong, X., et al.: A novel underactuated continuum robot with shape memory alloy clutches, IEEE/ASME Trans. Mechatronics, Vol. 27, No. 6, pp. 5339–5350, 2022.

[16] Dupont P.E., Simaan N., Choset H., Rucker C.: Continuum Robots for Medical Interventions, in: Proc. IEEE Inst. Electr. Electron. Eng., Vol. 110, No. 7, pp. 847–870, 2022.

[17] Ma N., Monk S., Cheneler D.: Collaborative Con–tinuum Robots for Remote Engineering Operations, Biomimetics (Basel), Vol. 8, No. 1, 2022.

[18] Onose R., Sawada H.: A Ball-Jointed Tendon-Dri–ven Continuum Robot with Multi-Directional Operability for Grasping Objects, Robomech J., Vol. 11, No. 4, pp. 1–10, 2024.

[19] Shi C., Luo X., Qi P., Li T., Song S., Najdovski Z., Fukuda T., Ren H.: Shape Sensing Techniques for Continuum Robots in Minimally Invasive Surgery: A Survey, IEEE Trans. Biomed. Eng., Vol. 64, No. 8, pp. 1665–1678, 2017.

[20] Godage, I.S., Guglielmino, E., Branson, D.T., et al.: Novel modal approach for kinematics of multi–section continuum arms, in: Proc. IEEE/RSJ Int. Conf. Intell. Robot. Syst., San Francisco, CA, USA, pp. 1093–1098, 2011.

[21] Jones, B.A., Walker, I.D.: Kinematics for multi–session continuum robots, IEEE Trans. Robot., Vol. 22, No. 1, pp. 43–55, 2006.

[22] He, B., Wang, Z., Li, Q., et al.: An analytic method for the kinematics and dynamics of a multiple-backbone continuum robot, Int. J. Adv. Robot. Syst., Vol. 10, No. 1, pp. 1–13, 2013.

[23] Renda, F., Boyer, F., Dias, J., et al.: Discrete Cos–serat approach for multisection soft manipulator dynamics, IEEE Trans. Robot., Vol. 34, No. 6, pp. 1518–1533, 2018.

[24] Mishra, M.K., Samantaray, A.K., Chakraborty, G., et al.: Kinematics model of bionic manipulator by using elliptic integral approach, in: Kumar, R., Chauhan, V.S., Talha, M., Pathak, H. (Eds.), Machines, Mechanism and Robotics, Lecture Notes Mech. Eng., Springer, Singapore, 2022.

[25] Hirose, S.: Biologically inspired robots, Oxford Univ. Press, Oxford, pp. 147–155, 1993.

[26] Hirose, S., Yamada, H.: Snake-like robots, IEEE Robot. Autom. Mag., Vol. 16, No. 1, pp. 88–98, 2009.

[27] Mohandes M. et al.: GARM: A Stochastic Evolution based Genetic Algorithm with Rewar–ding Mechanism for Wind Farm Layout Optimi–zation, FME Transactions, Vol. 51, No. 4, pp. 575–584, 2023.

[28] Rasha M.H.: Design a New Hybrid Controller Ba–sed on an Improvement Version of Grey Wolf Optimization for Trajectory Tracking of Wheeled Mobile Robot, FME Transactions, Vol. 51, No. 2, pp. 140–148, 2023.

[29] Alzaidi A.A., Al-Omari H.A., Al-Kadhem A.M.: Optimal Tuning of FOPID Controller Using Diffe–rential Search Algorithm for DC-DC Converter, FME Transactions, Vol. 50, No. 4, pp. 547–554, 2022.

[30] Hammad A., Khan S.A., Mahmood Z.: Modified Artificial Bee Colony Optimization Algorithm for Economic Load Dispatch Problem, FME Transactions, Vol. 49, No. 1, pp. 57–65, 2021.

[31] Shi, Y. and Eberhart, R.: A modified particle swarm optimizer, in: Proc. IEEE Int. Conf. Evol. Comput., IEEE World Congr. Comput. Intell., Anchorage, AK, USA, 1998.

[32] Webster III, R.J., Jones, B.A.: Design and kine–matic modeling of constant curvature continuum robots: a review, Int. J. Robot. Res., Vol. 29, No. 13, pp. 1661–1683, 2010.

[33] \Amouri, A., Cherfia, A., Merabti, H., Laib, D.L.Y.: Nonlinear model predictive control of a class of continuum robots using kinematic and dynamic models, FME Transactions, Vol. 50, No. 2, pp.339–350, 2022.

[34] Belkhiri, A., Amouri, A., Cherfia, A.: Design of Fractional-Order PID Controller for Trajectory Tracking Control of Continuum Robots, FME Transactions, Vol. 51, No. 2, pp. 243-252, 2023.

[35] Amouri, A., Laib Dit Leksir, Y., Merabti, H. et al.: Performance Evaluation of Particle Swarm Optimization Variants for Trajectory Tracking of a Cable-Driven Continuum Robot: Descriptive, Parametric, and Non-Parametric Statistical Analysis. Int J Adv Manuf Technol, Vol. 138, No. 2, pp. 603–615, 2025.

NOMENCLATURE

$c(\cdot)$	Cosine function.
c_1	Cognitive scaling factor.
c_2	Social scaling factor.
C_f	Objective function
H	Homogenous transformation matrix.
l_1,l_2,l_3	Actuation cable lengths
p	Particle.
R	Rotation matrix.
r	Radial distance between the virtual central axis of the SB-CDCR and the cables.
$s(\cdot)$	Sine function.
s	Arc length.
x	Position vector
x, y, z	Cartesian coordinates
G^{best}	Swarm best position
P^{best}	Personal best position
v_t^p	Current velocity of the particle p
x_t^p	Current position of the particle p

Greek symbols

θ	Bending angle
φ	Orientation angle
ω	Inertia weight.
ρ_1, ρ_2	Random numbers.

Abbreviations and Acronyms

ABC	Artificial Bee Colony
CC	Constant Curvature
CDCR	Cable-Driven Continuum Robot.
Conf_HB	Horizontal configuration with downward curvature.
Conf_HH	Horizontal configuration with upward curvature.
Conf_VB	Vertical configuration with the free end oriented downward.
Conf_VH	Vertical configuration with the free end oriented upward.
SB-CDCR	Self-Balancing Cable-Driven Continuum Robot.
DSA	Differential Search Algorithm
GA	Genetic Algorithm
GWO	Grey Wolf Optimization
W-PSO	Weighted Particle Swarm Optimization

ПРОЈЕКТОВАЊЕ, МОДЕЛИРАЊЕ И ВАЛИДАЦИЈА САМОБАЛАНСИРАЈУЋЕГ КОНТИНУУМ РОБОТА ПОКРЕТАНОГ КАБЛОМ КОРИСТЕЋИ УНУТРАШЊУ РАВНОТЕЖУ СИЛА

А. Амоури, О. Рахма

Обезбеђивање ефикасног рада је кључно за континуум роботе, посебно у задацима који захтевају прецизност под различитим спољашњим оптерећењима. Ова студија представља самобалансирајућег континуум робота покретаног каблом (SB-CDCR) дизајнираног да минимизира вибрације и побољша механичку стабилност, овде дефинисану као способност робота да одржи облик, одупре се деформацији и сузбије осцилације током кретања. Почетни дизајн робота састоји се од три модула, сваки састављен од суседних парова дискова међусобно повезаних са четири опруге: једна централна компресиона опруга за аксијалну потпору и три бочне затезне опруге за пасивно балансирање. Предложени дизајн интегрише неколико кључних карактеристика, укључујући лагану структуру, високу флексибилност и ојачану унутрашњу пот–пору. Ова конфигурација, у комбинацији са прет–ходно напрегнутом расподелом унутрашње силе, обезбеђује глатко кретање, сузбијање вибрација и побољшани структурни интегритет, чиме омогућава прецизну контролу просторних кретања. Кинема–тички модели су развијени коришћењем приступа константне закривљености (CC), што омогућава аналитичку формулацију директне кинематике и анализу радног простора. Инверзна кинематика се решава као задатак квадратне оптимизације и ефи–касно се решава коришћењем алгоритма оптими–зације роја пондерисаних честица (W-PSO). Нуме–ричке симулације демонстрирају прецизно праћење путање са позиционом грешком од 2,616×10□³ mm и временом израчунавања од ms. Експерименталне валидације додатно потврђују тачност робота у условима руковања теретом.